nature materials

LETTERS

https://doi.org/10.1038/s41563-019-0597-8

Selective nitrogen adsorption via backbonding in a metal–organic framework with exposed vanadium sites

David E. Jaramillo[1,7], Douglas A. Reed[1,7], Henry Z. H. Jiang[1], Julia Oktawiec[1], Michael W. Mara[1], Alexander C. Forse[1,2,3], Daniel J. Lussier[1,4], Ryan A. Murphy[1], Marc Cunningham[3], Valentina Colombo[5], David K. Shuh[4], Jeffrey A. Reimer[3,6] and Jeffrey R. Long[1,3,6*]

Industrial processes prominently feature π-acidic gases, and an adsorbent capable of selectively interacting with these molecules could enable important chemical separations[1–4]. Biological systems use accessible, reducing metal centres to bind and activate weakly π-acidic species, such as N_2, through backbonding interactions[5–7], and incorporating analogous moieties into a porous material should give rise to a similar adsorption mechanism for these gaseous substrates[8]. Here, we report a metal–organic framework featuring exposed vanadium(II) centres capable of back-donating electron density to weak π acids to successfully target π acidity for separation applications. This adsorption mechanism, together with a high concentration of available adsorption sites, results in record N_2 capacities and selectivities for the removal of N_2 from mixtures with CH_4, while further enabling olefin/paraffin separations at elevated temperatures. Ultimately, incorporating such π-basic metal centres into porous materials offers a handle for capturing and activating key molecular species within next-generation adsorbents.

The implementation of adsorbent-based technology is a promising route towards mitigating the high energy costs associated with current industrial chemical separations[1,2]. While most separation processes exploit volatility differences to impart selectivity, which requires energetically costly operating conditions, porous materials can separate gases based on chemical handles and thus can operate at more moderate pressures and temperatures[2]. However, current adsorbents typically distinguish adsorbates based on differences in polarizability, size or shape, and remain largely ineffective for mixtures that lack these particular distinctions. Many industrially relevant gases, such as H_2, N_2, O_2, alkenes, alkynes and CO, feature low-energy, π-symmetric orbitals capable of accepting electron density, but an adsorbent that effectively leverages this property for energy-efficient separations has not been realized. Designing a material with exposed metal sites capable of backbonding to adsorbates would introduce π acidity as a handle for imparting selectivity, enabling separations of industrially relevant mixtures.

Metal–organic frameworks have emerged as strong candidates for replacing traditional solid adsorbents[9–12]. These structures are built of metal nodes connected through multitopic organic linkers, and their surface functionalities can be chemically tuned to control adsorption properties. A prominent feature among metal–organic frameworks that offer superior adsorption characteristics is coordinatively unsaturated metal centres. Due to the typical metal ions and weak ligand field linkers used, this generally yields exposed Lewis-acidic metal sites that are capable of accepting electron density from various adsorbates and enables polarizability-based separations[13,14]. However, such materials cannot distinguish gases through backbonding. Separating mixtures where π acidity is a more suitable handle requires a material with exposed, reducing metal centres with the proper electron configuration that can donate electron density into an adsorbate π* orbital, as seen in nitrogenases and their biomimetic analogues[5–7]. A hypothetical metal–organic framework containing square-pyramidal vanadium(II) centres was previously proposed as an excellent candidate for backbonding-based separations[8]. Here, the electropositive and diffuse vanadium 3*d* orbitals promote an effective energetic and spatial overlap with the adsorbate π* lowest unoccupied molecular orbital, leading to a selective interaction over non-π acids. Additionally, the d^3 configuration in this ligand geometry promotes strong yet reversible backbonding interactions. However, many properties of vanadium(II), such as its kinetic inertness, susceptibility towards oxidation and reactivity with carboxylate-containing ligands[15], have prohibited the synthesis of a suitable material. Although some metal–organic frameworks contain metal centres with the appropriate electronic configuration for π backbonding, the lack of diffuse orbitals or the requisite molecular orbital energies has prevented realization of an effective adsorbent for π-acidic gases[16,17].

The importance of addressing these synthetic challenges is emphasized by considering one of the most industrially expensive separations: the removal of N_2 from natural gas[18,19]. Given their similar physical properties, separating N_2 and CH_4 is challenging and is currently carried out using capital- and energy-intensive cryogenic distillation. As the global energy market share of natural gas continues to increase, and as N_2-contaminated alternative sources of methane become more accessible, the development of an energy-efficient separation process is increasingly important[20]. While some N_2-selective adsorbents[17,21] and molecular solutions[22] exist, these suffer from either low equilibrium selectivity or low N_2 capacity and are therefore ineffective for large-scale applications. An adsorbent with a high density of square-pyramidal vanadium(II) sites

[1]Department of Chemistry, University of California, Berkeley, CA, USA. [2]Berkeley Energy and Climate Institute, University of California, Berkeley, CA, USA. [3]Department of Chemical and Biomolecular Engineering, University of California, Berkeley, CA, USA. [4]Chemical Sciences Division, Lawrence Berkeley National Laboratory, Berkeley, CA, USA. [5]Dipartimento di Chimica, Università di Milano, Milan, Italy. [6]Materials Sciences Division, Lawrence Berkeley National Laboratory, Berkeley, CA, USA. [7]These authors contributed equally: David E. Jaramillo, Douglas A. Reed. *e-mail: jrlong@berkeley.edu

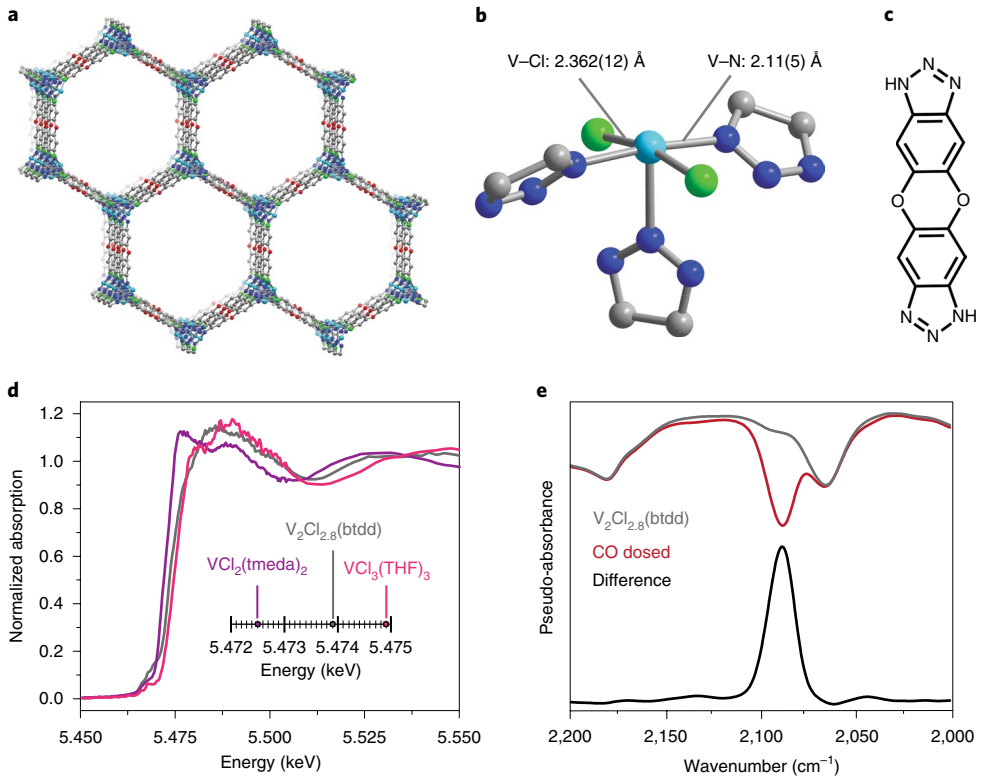

Fig. 1 | Structural and spectroscopic characterization of $V_2Cl_{2.8}$(btdd). a,**b**, Portion of the $V_2Cl_{2.8}$(btdd) structure (**a**), as determined from analysis of powder X-ray diffraction data, and a single five-coordinate vanadium centre within the framework (**b**). Cyan, green, blue, red and grey spheres represent V, Cl, N, O and C, atoms respectively. Terminal chloride ligands and H atoms have been omitted for clarity. **c**, Structure of the organic linker H_2btdd. **d**, Vanadium K-edge X-ray absorption spectra collected for $V_2Cl_{2.8}$(btdd) (grey), a vanadium(II) reference V_2Cl_2(tmeda)$_2$ (purple) and a vanadium(III) reference $VCl_3(THF)_3$ (pink). The inset depicts edge energies determined at the half-maximum of the rising edge (Supplementary Table 1). **e**, Infrared spectra collected at 25 °C for activated $V_2Cl_{2.8}$(btdd) (grey) and $V_2Cl_{2.8}$(btdd) dosed with 33 mbar of CO (red), with the difference between these two spectra shown in black.

could overcome these limitations by exploiting the π acidity of N_2. Herein, we report the synthesis of a metal–organic framework with exposed vanadium(II) sites, $V_2Cl_{2.8}$(btdd) (H_2btdd, bis(1*H*-1,2,3-triazolo[4,5-*b*],[4′,5′-*i*])dibenzo[1,4]dioxin), which engages π-acidic gases via backbonding interactions. This material exhibits a record N_2 capacity under practical working conditions, a record equilibrium selectivity for N_2 over CH_4 and facile regeneration, qualifying it as a potential candidate for natural gas purification. Furthermore, this backbonding capability can be leveraged to separate olefins from paraffins, another energy-demanding industrial separation[1,4]. Importantly, this discovery expands the molecular properties that can be targeted by solid adsorbents to discriminate gases in industrial processes.

The M_2Cl_2(btdd) structure type was identified as a promising target to synthesize a vanadium(II)-based metal–organic framework[23]. The nitrogen donors of the btdd^{2-} ligand avoid the deleterious vanadium oxidation reactions observed with more common carboxylate-containing ligands[15]. Additionally, using a vanadium chloride precursor should minimize the rearrangement required of the metal coordination sphere, partially circumventing the kinetic inertness of vanadium(II). Indeed, combining VCl_2(tmeda)$_2$ (tmeda, *N*,*N*,*N*′,*N*′-tetramethylethylenediamine) and H_2btdd (Fig. 1c) in *N*,*N*-dimethylformamide under acidic conditions affords a dark purple microcrystalline powder. The activated material is highly porous, with a Brunauer–Emmett–Teller surface area of 1,930 $m^2 g^{-1}$, and Rietveld refinement of powder X-ray diffraction (PXRD) data yielded a structural model consistent with the formula $V_2Cl_{2.8}$(btdd) (Fig. 1a and Supplementary Figs. 1 and 2). The framework features one-dimensional, hexagonal channels with vertices decorated by vanadium sites. Due to the highly reducing nature of vanadium(II), some of the metal sites are oxidized during synthesis, resulting in a framework containing approximately 60% coordinatively unsaturated vanadium(II) sites (Fig. 1b) and 40% coordinatively saturated, chloride-terminated vanadium(III) sites (Supplementary Fig. 3). This metal site distribution was validated by vanadium K-edge X-ray absorption spectroscopy, which revealed an edge energy consistent with the presence of a mixture of vanadium(II) and vanadium(III) (Fig. 1d), and X-ray photoelectron spectroscopy, which indicated the presence of both bridging and terminal chloride ligands (Supplementary Fig. 4). All vanadium centres are coordinated by bridging triazolates and chlorides, with V–N bond lengths ranging from 2.11(5) to 2.29(13) Å, and equatorial V–Cl bond distances of 2.362(12) Å, consistent with mixed vanadium(II)/vanadium(III) character[24,25].

To confirm the accessibility and electron-donating ability of the square-pyramidal vanadium(II) centres, a sample dosed with CO was monitored with in situ infrared spectroscopy. After CO dosing a single band appears at 2,084 cm^{-1}, indicating the presence of only one type of vanadium binding site (Fig. 1e). The band is weakly redshifted by 59 cm^{-1} from that of free CO, in contrast to the blueshift observed in the majority of frameworks that bind adsorbates via a Lewis-acidic mechanism[13,17]. Even frameworks with metal centres that were proposed to operate through a backbonding mechanism, such as those containing square-pyramidal chromium(III) sites, act as Lewis acids and exhibit blueshifted C–O stretching frequencies[17]. This result clearly demonstrates that a backbonding interaction is

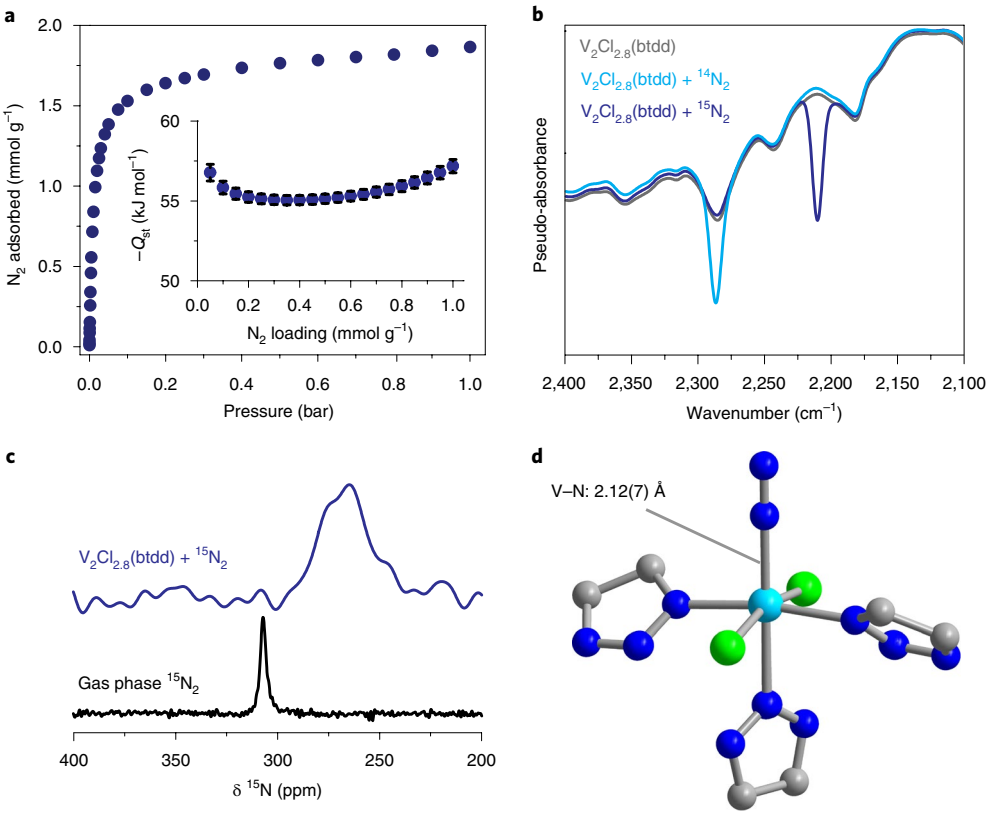

Fig. 2 | Characterization of the V–N_2 interaction in $V_2Cl_{2.8}$(btdd). a, Nitrogen adsorption isotherm collected at 25 °C, with inset showing the isosteric heat of N_2 adsorption (error bars are shown in black). **b**, Infrared spectra for $V_2Cl_{2.8}$(btdd) collected at 25 °C under vacuum (grey), after dosing with 80 mbar of $^{14}N_2$ (cyan) and after dosing with 85 mbar of $^{15}N_2$ (blue). **c**, Nitrogen-15 nuclear magnetic resonance (NMR) spectra collected for free, gas-phase $^{15}N_2$ at 700 mbar (black) and for $V_2Cl_{2.8}$(btdd) dosed with 770 mbar of $^{15}N_2$ (blue) at room temperature. The spectrum of the solid sample was collected using magic-angle spinning at 15 kHz. **d**, Structure of a single vanadium site in $V_2Cl_{2.8}$(btdd) after dosing with 700 mbar of N_2, as determined from analysis of powder X-ray diffraction data. Cyan, green, blue and grey spheres represent V, Cl, N and C atoms, respectively; a 40%-occupied terminal chloride ligand has been omitted.

operating in $V_2Cl_{2.8}$(btdd) and suggests that the material should strongly adsorb other π-acidic substrates, such as N_2.

Indeed, $V_2Cl_{2.8}$(btdd) adsorbs substantial amounts of N_2 at ambient temperature. Equilibrium N_2 uptake at 25 °C exhibits an unprecedented steep rise to 1.5 mmol g^{-1} at just 50 mbar, before increasing to 1.9 mmol g^{-1} (>5 wt%) at 1 bar (Fig. 2a). Analysis of adsorption data afforded an isosteric heat of adsorption of −56 kJ mol^{-1}, the largest value reported for a porous material exhibiting reversible N_2 binding. This is consistent with the computationally predicated value of −49 kJ mol^{-1} for the hypothetical material V_2(dobdc) (dobdc^{4-}, 2,5-dioxido-1,4-benzenedicarboxylate)[8].

The N_2 adsorption mechanism in $V_2Cl_{2.8}$(btdd) was probed through a variety of techniques. Analysis of PXRD data collected on a sample dosed with N_2 revealed a linear, end-on binding mode for N_2 with a V–N separation of 2.12(7) Å (Fig. 2d). This bond distance is the shortest metal–N_2 interaction reported amongst metal–organic frameworks[8,26], and represents the first structurally characterized example of μ_1-N_2–vanadium(II). Nitrogen adsorption in $V_2Cl_{2.8}$(btdd) was also monitored using in situ infrared spectroscopy (Fig. 2b). After dosing N_2, a single, isotopically sensitive N–N stretching band appears at 2,290 cm^{-1}. This value is redshifted by 41 cm^{-1} relative to gas-phase N_2, consistent with a computationally predicted weak field vanadium(II)–N_2 interaction, free of solvent and cation effects[8]. Finally, solid-state magic-angle spinning ^{15}N-NMR spectroscopy data were collected for a $V_2Cl_{2.8}$(btdd) sample dosed with $^{15}N_2$ (Fig. 2c). The signal observed at 267 ppm was notably broadened and paramagnetically shifted from free, gas-phase N_2 (307 ppm), in contrast to what is observed in Lewis-acidic adsorbents[27] and consistent with the transfer of unpaired electron spin density from vanadium to N_2. Together, these data confirm that N_2 binding at the vanadium centres involves a π-backbonding interaction.

The substantial N_2 uptake resulting from this binding mechanism should enable exceptional performance in industrial applications. Removing N_2 from mixtures with CH_4, one of the largest commercial separations involving N_2, is necessary for processing contaminated natural gas reserves. Pipeline quality standards require a total inert gas content of less than 4%, with N_2 levels typically below 2% (refs. [3,19,20]). Consequently, a viable adsorbent must maximize both capacity and selectivity for N_2 over CH_4 at low N_2 partial pressures. A comparison of $V_2Cl_{2.8}$(btdd) with previously reported materials for N_2 capture[17,21] reveals that the backbonding adsorption mechanism allows for the highest uptake at near-ambient temperatures. In particular, the performance of $V_2Cl_{2.8}$(btdd) at low pressures far surpasses any previously reported value. The previous benchmark material, a chromium(III) metal–organic framework, adsorbs ~0.25 mmol g^{-1} at 20 mbar at 10 °C (ref. [17]), compared with 1.09 mmol g^{-1} at 20 mbar observed for $V_2Cl_{2.8}$(btdd) at the higher temperature of 25 °C. Importantly, even with this substantial uptake, the weak π-backbonding mechanism results in fully reversible N_2 adsorption, as shown through successive adsorption/desorption cycles that show no loss in capacity (Fig. 3c).

In assessing the N_2 adsorption selectivity, a comparison with the CH_4 adsorption isotherm collected at 25 °C shows that

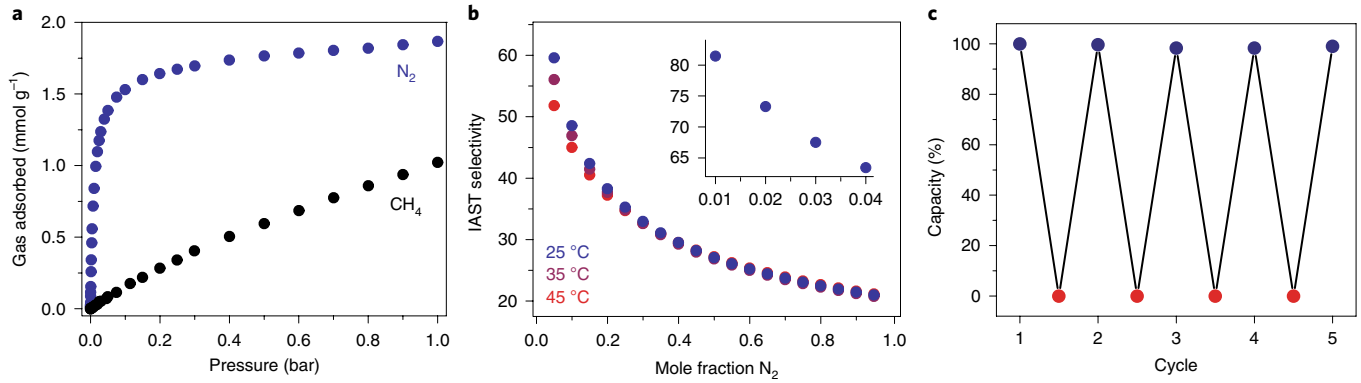

Fig. 3 | Assessment of N_2/CH_4 selectivity and N_2 adsorption reversibility. a, Adsorption isotherms for N_2 (blue) and CH_4 (black) collected at 25 °C in $V_2Cl_{2.8}$(btdd). **b**, IAST selectivity values calculated at 25, 35 and 45 °C for varying N_2:CH_4 ratios at a total pressure of 1 bar. The inset highlights the IAST selectivity values at low N_2 concentrations. **c**, Cycling data for successive N_2 adsorption and desorption. Adsorption capacities are expressed in terms of percentage of uptake relative to the first cycle. Adsorption (blue circles) was collected at 25 °C and 1 bar. Desorption (red circles) occurred by applying dynamic vacuum at 50 °C for 10 min.

$V_2Cl_{2.8}$(btdd) adsorbs substantially more N_2 below 1 bar (Fig. 3a). While $V_2Cl_{2.8}$(btdd) adsorbs CH_4 with a considerable binding enthalpy of −35 kJ mol^{-1}, similar to that predicted for V_2(dobdc) (ref. [8]), its adsorption profile relative to that of N_2 suggests that the framework should selectively bind N_2. Indeed, N_2/CH_4 selectivity values calculated using ideal adsorbed solution theory (IAST) are exceptional for low N_2 concentrations at 1 bar total pressure (Fig. 3b). For example, for a 20:80 N_2:CH_4 mixture at 25 °C, the selectivity is 38. This value is substantially higher than the selectivity of ~8 reported for the previous benchmark material, which is reported at 10 °C and decreases considerably on warming[17]. Notably, due to the steep rise in the N_2 adsorption isotherm in $V_2Cl_{2.8}$(btdd), the IAST selectivity rises substantially at lower concentrations of N_2, reaching a value of 72 at 2:98 N_2:CH_4. Furthermore, the material selectively adsorbs CO_2, another key contaminant in many sources of natural gas[3], over CH_4, with an IAST value of 37 for the industrially relevant 10:90 CO_2:CH_4 mixture (Supplementary Fig. 5). This suggests that $V_2Cl_{2.8}$(btdd) should be capable of removing both N_2 and CO_2 from crude natural gas in a single-pass separation process.

Importantly, N_2 adsorption isotherms remain steep at higher temperatures, indicating that $V_2Cl_{2.8}$(btdd) should be selective for N_2/CH_4 separations even at substantially elevated temperatures (Supplementary Figs. 6 and 7). For temperatures as high as 45 °C, the IAST selectivity values are similar to those calculated at 25 °C and remain practically invariant at N_2 concentrations higher than 20% over this temperature range (Fig. 3b), highlighting the importance of the strong orbital-mediated V–N_2 interaction. This result is analogous to that observed for other materials that form strong, chemisorptive interactions with target substrates[28]. In contrast, polarizability driven mechanisms exhibit dramatic negative temperature effects, which is observed in the previous benchmark chromium(III) material, where raising the temperature from 10 to 20 °C lowers the IAST selectivity under standard conditions by over 20% (ref. [17]).

We sought to investigate the applicability of this backbonding adsorption mechanism to the separation of olefins from paraffins, which operates on enormous scales using cryogenic distillation[1,4]. Metal–organic frameworks containing coordinatively unsaturated metal centres have previously been studied for the separation of ethylene/ethane and propylene/propane[11,29]. However, while these materials perform effectively at room temperature, their selectivity diminishes substantially at the higher temperatures that can align with olefin/paraffin production processes[4,30]. We monitored the mechanism of olefin adsorption in $V_2Cl_{2.8}$(btdd) by in situ dosing

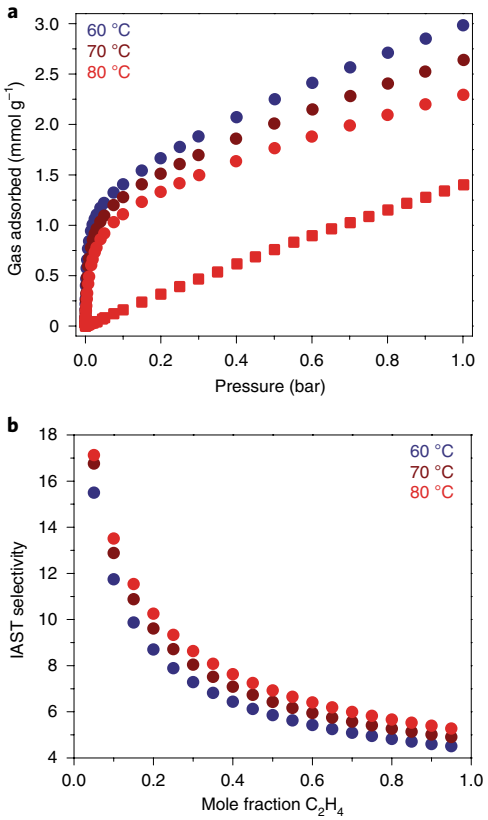

Fig. 4 | Selective ethylene capture at high temperatures. a, High-temperature ethylene and ethane adsorption isotherms collected at various temperatures for $V_2Cl_{2.8}$(btdd). Circles and squares represent ethylene and ethane isotherms, respectively. **b**, IAST selectivity values calculated at 60, 70 and 80 °C for varying ethylene:ethane ratios at a total pressure of 1 bar.

of propylene while collecting infrared spectra. The room-temperature spectrum features a redshifted C=C stretch at 1,620 cm^{-1} (Supplementary Fig. 8), suggestive of a backbonding interaction with the olefin π^* orbitals. Analysis of ethylene and propylene adsorption isotherms further reveals that both gases adsorb with similar binding enthalpies of −68 and −67 kJ mol^{-1}, respectively (Supplementary Fig. 9 and Supplementary Table 2). These results

again support a backbonding adsorption mechanism, in contrast to traditional Lewis-acidic binding sites that operate via a polarizability-based mechanism and bind propylene more strongly than ethylene[11].

Due to π backbonding, $V_2Cl_{2.8}$(btdd) retains strong binding affinities for olefins at high temperatures. Indeed, the ethylene adsorption isotherm collected at 80 °C shows a steep and substantial uptake, and, notably, the adsorption remains fully reversible even at lower temperatures (Fig. 4a and Supplementary Fig. 10). In contrast, ethane adsorption isotherms are more shallow at all temperatures measured. For a 50:50 ethylene:ethane mixture, the IAST selectivity notably increases with temperature, reaching a value of 6.9 at 80 °C (Fig. 4b). This instance of selectivity increasing with temperature for this industrially relevant mixture could allow for operation under much more energetically favourable conditions[4,30]. Additionally, the record ethylene selectivity values exhibited by the framework at elevated temperatures and low ethylene concentrations—17 for a 5:95 ethylene:ethane mixture at 80 °C—suggest that this material may be particularly effective for the separation of ethylene in ethane-rich feeds.

Realization of a material with reducing, coordinatively unsaturated vanadium(II) centres capable of strong yet reversible backbonding interactions has unleashed an extraordinary potential for binding of π-acidic gases. Indeed, $V_2Cl_{2.8}$(btdd) exemplifies valuable design principles for next-generation adsorbents capable of exploiting differences in adsorbate molecular orbitals to impart selectivity and, potentially, even new reactivity that has yet to be explored.

Online content

Any methods, additional references, Nature Research reporting summaries, source data, extended data, supplementary information, acknowledgements, peer review information; details of author contributions and competing interests; and statements of data and code availability are available at https://doi.org/10.1038/s41563-019-0597-8.

Received: 31 May 2019; Accepted: 18 December 2019;
Published online: 3 February 2020

References

1. Sholl, D. S. & Lively, R. P. Seven chemical separations to change the world. *Nature* **532**, 435–438 (2016).
2. *Materials Separation Technology: Energy and Emission Reduction Opportunities* (US Department of Energy, 2005).
3. Rufford, T. E. et al. The removal of CO_2 and N_2 from natural gas: a review of conventional and emerging process technologies. *J. Pet. Sci. Eng.* **94**, 123–154 (2012).
4. Eldridge, R. B. Olefin/paraffin separation technology: a review. *Ind. Eng. Chem. Res.* **32**, 2208–2212 (1993).
5. Hoffman, B. M., Lukoyanov, D., Yang, Z.-Y., Dean, D. R. & Seefeldt, L. C. Mechanism of nitrogen fixation by nitrogenase: the next stage. *Chem. Rev.* **114**, 4041–4062 (2014).
6. Crans, D. C., Smee, J. J., Gaidamauskas, E. & Yang, L. The chemistry and biochemistry of vanadium and the biological activities exerted by vanadium compounds. *Chem. Rev.* **104**, 840–902 (2004).
7. MacKay, B. A. & Fryzuk, M. D. Dinitrogen coordination chemistry: on the biomimetic borderlands. *Chem. Rev.* **104**, 385–402 (2004).
8. Lee, K. et al. Design of a metal–organic framework with enhanced back bonding for separation of N_2 and CH_4. *J. Am. Chem. Soc.* **136**, 698–704 (2014).
9. Furukawa, H., Cordova, K. E., O'Keefe, M. & Yaghi, O. M. The chemistry and applications of metal–organic frameworks. *Science* **341**, 1230444 (2013).
10. Li, J. R., Kuppler, R. J. & Zhou, H. C. Selective gas adsorption and separation in metal–organic frameworks. *Chem. Soc. Rev.* **38**, 1477–1504 (2009).
11. Bloch, E. D. et al. Hydrocarbon separations in a metal–organic framework with open iron(II) sites. *Science* **335**, 1606–1610 (2012).
12. Cadieu, A., Adil, K., Bhatt, P. M., Belmabkhout, Y. & Eddaoudi, M. A metal–organic framework-based splitter for separating propylene from propane. *Science* **353**, 137–140 (2016).
13. Lee, K., Howe, J. D., Lin, L.-C., Smit, B. & Neaton, J. B. Small-molecule adsorption in open-site metal–organic frameworks: a systematic density functional theory study for rational design. *Chem. Mater.* **27**, 668–678 (2015).
14. Poloni, R., Lee, K., Berger, R. F., Smit, B. & Neaton, J. B. Understanding trends in CO_2 adsorption in metal–organic frameworks with open-metal sites. *J. Phys. Chem. Lett.* **5**, 861–865 (2014).
15. Cotton, F. A. et al. Four compounds containing oxo-centered trivanadium cores surrounded by six μ,η^2-carboxylato groups. *Inorg. Chem.* **25**, 3505–3512 (1986).
16. Denysenko, D., Grzywa, M., Jelic, J., Reuter, K. & Volkmer, D. Scorpionate-type coordination in MFU-4*l*metal–organic frameworks: small-molecule binding and activation upon the thermally activated formation of open metal sites. *Angew. Chem. Int. Ed. Engl.* **53**, 5832–5836 (2014).
17. Yoon, J. W. et al. Selective nitrogen capture by porous hybrid materials containing accessible transition metal ion sites. *Nat. Mater.* **16**, 526–531 (2017).
18. Caventi, S., Grande, C. A. & Rodrigues, A. E. Separation of $CH_4/CO_2/N_2$ mixtures by layered pressure swing adsorption for upgrade of natural gas. *Chem. Eng. Sci.* **61**, 3893–3906 (2006).
19. Lokhandwala, K. A. et al. Membrane separation of nitrogen from natural gas: a case study from membrane synthesis to commercial deployment. *J. Membr. Sci.* **346**, 270–279 (2010).
20. Saha, D., Grappe, H. A., Chakraborty, A. & Orkoulas, G. Postextraction, separation, on-board storage, and catalytic conversion of methane in natural gas: a review. *Chem. Rev.* **116**, 11436–11499 (2016).
21. Kuznicki, S. M. et al. A titanosilicate molecular sieve with adjustable pores for size-selective adsorption of molecules. *Nature* **412**, 720–724 (2004).
22. Bartholomew, E. R., Volpe, E. C., Wolczanski, P. T., Lobkovsky, E. B. & Cundari, T. R. Selective extraction of N_2 from air by diarylamine iron complexes. *J. Am. Chem. Soc.* **135**, 3511–3527 (2013).
23. Rieth, A. J., Tulchinsky, Y. & Dincă, M. High and reversible ammonia uptake in mesoporous metal–organic frameworks with open Mn, Co, and Ni sites. *J. Am. Chem. Soc.* **138**, 9401–9404 (2016).
24. Bechlars, B. et al. High-spin ground states via electron delocalization in mixed-valence imidazolate-bridged divanadium complexes. *Nat. Chem.* **2**, 362–368 (2010).
25. Cotton, F. A. et al. Structural studies of the vanadium(II) and vanadium(III) chloride tetrahydrofuran solvates. *J. Chem. Soc. Chem. Commun.* **23**, 1377–1378 (1983).
26. Gonzalez, M. I. et al. Structural characterization of framework-gas interactions in the metal–organic framework Co_2(dobdc) by *in situ* single-crystal X-ray diffraction. *Chem. Sci.* **8**, 4387–4398 (2017).
27. Fonseca, A., Lledos, B., Pullumbi, P., Lignieres, J. & Nagy, J. B. ^{15}N-NMR characterization and quantitative NMR determination of nitrogen adsorbed in MX zeolites. *Surf. Sci. Catal.* **125**, 229–236 (1999).
28. Reed, D. A. et al. Reversible CO scavenging via adsorbate-dependent spin state transitions in an iron(II)–triazolate metal–organic framework. *J. Am. Chem. Soc.* **138**, 5594–5602 (2016).
29. Li, B. et al. Introduction of pi-complexation into porous aromatic framework for highly selective adsorption of ethylene over ethane. *J. Am. Chem. Soc.* **136**, 8654–8660 (2014).
30. Ren, T., Patel, M. & Blok, K. Olefins from conventional and heavy feedstocks: energy use in steam cracking and alternative processes. *Energy* **31**, 425–451 (2006).

Methods

General synthesis and characterization methods. The metal–organic framework synthesis, washing and activation were adapted, as described below, from established methods[31]. The crystal structure and gas adsorption properties were characterized as previously described[31], and are reported below for completeness. All synthetic procedures were performed under an argon atmosphere using standard Schlenk techniques or in an N_2-filled VAC Atmospheres glovebox. Methanol was purchased from EMD Millipore as DriSolv grade, dried over 3-Å molecular sieves, and sparged with argon before use. *N,N*-Dimethylformamide (DMF) was purchased from EMD Millipore as OmniSolv grade, sparged with argon and dried with an alumina column before use. The materials $VCl_2(tmeda)_2$, $H_2(btdd)$ and $VCl_3(THF)_3$ (THF, tetrahydrofuran) were prepared according to previously reported procedures[32–34]. Dimethylformamidium trifluoromethanesulfonate was purchased from Sigma-Aldrich and dried under vacuum before use. Ultrahigh purity-grade (99.999%) He, N_2, CH_4 and CO_2, and research purity grade (99.99%) CO, C_2H_4, C_2H_6 and C_3H_6 were used for all gas adsorption measurements and dosing. Isotopically labelled $^{15}N_2$ (98 atom% ^{15}N) was purchased from Sigma-Aldrich and used as received. Elemental analyses for C, H and N were performed at the Microanalytical Laboratory at the University of California, Berkeley.

Synthesis of $V_2Cl_{2.8}(btdd)$. A solution of $VCl_2(tmeda)_2$ (90.0 mg, 0.254 mmol) and dimethylformamidium trifluoromethanesulfonate (266 mg, 1.20 mmol) in DMF (10 ml) was added to a 20-ml borosilicate vial containing $H_2(btdd)$ (20.0 mg, 0.0752 mmol). The mixture was heated at 120 °C, without stirring, for 10 d. The resulting dark purple powder was collected by filtration, and soaked in 10 ml of DMF at 120 °C for 24 h. The supernatant solution was decanted, another 10 ml of DMF was added and the vial was heated at 120 °C for 24 h. This process was repeated five more times so that the total time washing with DMF was 7 d. The solid was then collected by filtration, and soaked in 10 ml of methanol at 60 °C for 12 h. The supernatant solution was decanted, and the remaining powder was soaked in another 10 ml of methanol at 60 °C for 12 h. This process was repeated four more times so that the total time washing with methanol was 3 d. The resulting solid was collected by filtration, and heated at a rate of 0.2 °C min^{-1} and held at 180 °C under dynamic vacuum for 36 h, affording 20 mg of product as a dark purple powder. Elemental analysis of $[V_2Cl_{2.8}(btdd)](CH_3OH)_2$, $C_{14}H_{12}Cl_{2.8}N_6O_4V_2$: Found C, 32.76; H, 2.44; N, 15.88. Calculated: C, 31.76; H, 2.28; N, 15.87.

Gas adsorption measurements. Gas adsorption isotherms for pressures in the range 0–1 bar were measured by a volumetric method using a Micromeritics ASAP 2020 or Micromeritics 3Flex gas sorption analyser. In an N_2-filled glovebox, a typical sample of approximately 50 mg was transferred to a pre-weighed analysis tube, which was capped with a Micromeretics TranSeal and evacuated by heating at 180 °C with a ramp rate of 0.2 °C min^{-1} under dynamic vacuum until an outgas rate of less than 3 μbar min^{-1} was achieved. The evacuated analysis tube containing the degassed sample was then carefully transferred to an electronic balance and weighed again to determine the mass of the sample. The tube was then transferred back to the analysis port of the gas adsorption instrument. The outgas rate was again confirmed to be less than 3 μbar min^{-1}. For all isotherms, warm and cold free-space correction measurements were performed using ultrahigh purity He gas. Isotherms of N_2, CH_4, CO_2, C_2H_4, C_2H_6 and C_3H_6 collected at 298–358 K were measured in water baths equipped with a Julabo F32 circulator. Isotherms of N_2 collected at 77 K were measured in liquid nitrogen baths. Oil-free vacuum pumps and oil-free pressure regulators were used for all measurements to prevent contamination of the samples during the evacuation process, or of the feed gases during the isotherm measurements. Langmuir surface areas were determined from N_2 adsorption data at 77 K using Micromeritics software.

Powder X-ray diffraction. Microcrystalline powder samples of $V_2Cl_{2.8}(btdd)$ (~5 mg) were loaded into two 1.0-mm boron-rich glass capillaries inside a glovebox under an N_2 atmosphere. The capillaries were attached to a gas cell, which was connected to the analysis port of a Micromeritics ASAP 2020 gas adsorption instrument. Both capillaries were fully evacuated at 180 °C for 12 h, one was then flame sealed while the other capillary was dosed with N_2 to a pressure of 700 mbar, equilibrated for 2 h and then flame sealed. Each capillary was placed inside a Kapton tube that was sealed on both ends with epoxy resin.

High-resolution synchrotron X-ray powder diffraction data were collected at Beamline 17-BM at the Advanced Photon Source at Argonne National Laboratory. The temperature of measurement of the capillary samples was kept at 298 K using an Oxford Cryosystems Cryostream 800. Scattered intensity was measured by a PerkinElmer a-Si flat panel detector. The average wavelength of all measurements was 0.45236 Å.

Infrared spectroscopy. Infrared spectra were collected using a Bruker Vertex 70 spectrometer equipped with a glowbar source, KBr beam splitter and a liquid nitrogen-cooled mercury–cadmium–telluride detector. A custom-built diffuse reflectance system with a infrared-accessible gas-dosing cell was used for all measurements. Sample temperature was controlled by an Oxford Instruments OptistatDry TLEX cryostat, and sample atmosphere was controlled by a Micromeritics ASAP 2020Plus gas sorption analyser. Before measurement, activated $V_2Cl_{2.8}(btdd)$ (10 wt%) was dispersed in dry KBr in an argon-filled glovebox and evacuated at room temperature for 30 min. Spectra were collected in situ under ultrahigh purity grade CO, N_2, propylene and $^{15}N_2$ (98 atom% ^{15}N, Sigma-Aldrich) at 4 cm^{-1} resolution continually until equilibrium was observed.

Solid-state NMR spectroscopy. NMR spectra were collected for free gas-phase $^{15}N_2$ (98 atom% ^{15}N, Sigma-Aldrich) and $^{15}N_2$-dosed $V_2Cl_{2.8}(btdd)$. For free, gas-phase $^{15}N_2$, the gas was dosed into an empty 4-mm outer diameter glass tube at 700 mbar and then flame sealed. Gas dosing for $V_2Cl_{2.8}(btdd)$ was performed on a custom gas-dosing manifold described previously[35]. The rotor was packed with ~30 mg of $V_2Cl_{2.8}(btdd)$ inside an N_2-filled glovebox, evacuated at room temperature for 30 min and then dosed with 773 mbar of $^{15}N_2$ at room temperature with 30 min allowed for equilibration. For the measurement collection, all NMR spectra were recorded at 16.4 T, with a Bruker 3.2-mm magic-angle spinning probe used for $^{15}N_2$-dosed $V_2Cl_{2.8}(btdd)$ and a Doty 4-mm magic-angle spinning probe used for the free gas-phase $^{15}N_2$ sample. For free $^{15}N_2$ the sample was static during measurement, while $^{15}N_2$-dosed $V_2Cl_{2.8}(btdd)$ was collected under magic-angle spinning at a rate of 15 kHz. Single pulse excitation was used for all NMR experiments. All spectra were referenced to ^{15}N in glycine with a chemical shift of 33.4 ppm (ref. [36]).

Vanadium K-edge X-ray absorption spectroscopy. Data were collected at the Advanced Light Source bending magnet microprobe beamline 10.3.2 (2.1–17 keV) with the storage ring operating at 500 mA and 1.9 GeV. The $V_2Cl_{2.8}(btdd)$, $VCl_2(tmeda)_2$ and $VCl_3(THF)_3$ samples were all individually mounted under inert atmosphere conditions in an argon glovebox onto Kapton tape, sealed in multiple hermetic bags, transferred to the Advanced Light Source and measured in fluorescence mode by continuously scanning the Si(111) monochromator (Quick XAS mode). Fluorescence emission counts were recorded with a seven-element Ge solid-state detector (Canberra) and XIA electronics. All spectra were collected from 100 eV below and up to 300 eV above the edge, and calibrated using a vanadium foil, with first derivative set at 5,465.1 eV. All data were processed using LabVIEW custom software available at the beamline and further processed with Athena[37].

X-ray photoelectron spectroscopy. X-ray photoelectron spectroscopy (XPS) data were taken using a PerkinElmer PHI 5600 XPS instrument. The XPS instrument was equipped with a 180° double focusing hemispherical analyser. To prevent oxygen contamination and concomitant redox activity with samples, preparation and mounting were performed in an argon glovebox. The sample was affixed to a silicon wafer using double-sided carbon tape. After mounting the wafer on the stage the sample was sealed in an airtight jar under argon. To load into the XPS, a glovebag containing the jar was sealed onto the loading chamber and subsequently purged with a high flow of argon for 1 h, after which the sample was loaded into the chamber under argon.

Samples were calibrated using the aromatic carbon peak as a standard. For proper peak fitting, a Shirley background was applied to regions of interest and subtracted after peak fitting. Energy splitting of spin–orbit decoupled peaks was constrained using values obtained from VCl_2 and VCl_3 standards. All data processing and peak fitting was performed using CasaXPS.

Data availability

The supplementary materials contain complete experimental and spectral details for all new compounds reported herein. Crystallographic data are available free of charge from the Cambridge Crystallographic Data Centre (CCDC). The CCDC numbers for the activated structure and for the N_2-dosed structure are 1971589 and 1971588, respectively.

References

31. Reed, D. A. et al. A spin transition mechanism for cooperative adsorption in metal–organic frameworks. *Nature* **550**, 96–100 (2017).
32. Edema, J. J. H. et al. Novel vanadium(II) amine complexes: a facile entry in the chemistry of divalent vanadium. Synthesis and characterization of mononuclear L_4VCl_2 [L=amine, pyridine]: X-ray structures of *trans*-$(TMEDA)_2VCl_2$ [TMEDA=*N,N,N′,N′*-tetramethylethylenediamine] and *trans*-$Mz_2V(py)_2$ [Mz=*o*-$C_6H_4CH_2N(CH_3)_2$, py=pyridine]. *Inorg. Chem.* **29**, 1302–1306 (1990).
33. Denysenko, D. et al. Elucidating gating effects for hydrogen sorption in MFU-4-type triazolate-based metal–organic frameworks featuring different pore sizes. *Chem. Eur. J.* **17**, 1837–1848 (2011).
34. Manzer, L. E., Deaton, J., Sharp, P. & Schrock, R. R. Tetrahydrofuran complexes of selected early transition metals. *Inorg. Synth.* **21**, 135–140 (1982).
35. Milner, P. J. et al. A diaminopropane-appended metal–organic framework enabling efficient CO_2 capture from coal flue gas via a mixed adsorption mechanism. *J. Am. Chem. Soc.* **139**, 13541–13553 (2017).

36. Bertani, P., Raya, J. & Bechinger, B. ^{15}N chemical shift referencing in solid state NMR. *Solid State Nucl. Magn. Reson.* **61**, 15–18 (2014).
37. Ravel, B. & Newville, B. M. ATHENA, ARTEMIS, HEPHAESTUS: data analysis for X-ray absorption spectroscopy using IFEFFIT. *J. Synchrotron Radiat.* **12**, 537–541 (2005).

Acknowledgements

The views and opinions of the authors expressed herein do not necessarily state or reflect those of the United States Government or any agency thereof. Neither the United States Government nor any agency thereof, nor any of their employees, makes any warranty, expressed or implied, or assumes any legal liability or responsibility for the accuracy, completeness, or usefulness of any information, apparatus, product, or process disclosed, or represents that its use would not infringe privately owned rights. The synthesis of $V_2Cl_{2.8}$(btdd) was supported by the Hydrogen Materials—Advanced Research Consortium (HyMARC), established as part of the Energy Materials Network under the US Department of Energy (DoE), Office of Energy Efficiency and Renewable Energy, Fuel Cell Technologies Office, under contract number DE-AC02-05CH11231, while its characterization by gas adsorption analysis, X-ray diffraction, infrared spectroscopy and NMR spectroscopy was supported by the US Department of Energy (DoE), Office of Science, Office of Basic Energy Sciences under award number DE-SC0019992. X-ray absorption spectroscopy experiments were supported by the Director, Office of Science, Office of Basic Energy Sciences, Division of Chemical Sciences, Geosciences, and Biosciences Heavy Elements Chemistry programme of the US DoE under contract number DE-AC02-05CH11231 (D.J.L. and D.K.S.), as well as the US DoE, Office of Science, Office of Basic Energy Sciences under award number DE-SC0016961 (M.W.M.), and data were collected with the X-ray absorption spectroscopy user resources of the Advanced Light Source, which is a DoE Office of Science User Facility under contract number DE-AC02-05CH11231. Powder X-ray diffraction data were collected at Beamline 17-BM at the Advanced Photon Source, a DoE Office of Science User Facility, operated by Argonne National Laboratory under contract number DE-AC02-06CH11357. We thank the National Science Foundation for graduate fellowship support of D.E.J., D.A.R. and J.O., the Philomathia Foundation and Berkeley Energy and Climate Institute for postdoctoral fellowship support of A.C.F. and Fondazione Banca del Monte di Lombardia - Progetto Professionalità Ivano Becchi 2016–2017 and University of Milan PSR 2017 for support of V.C. We are further grateful to the staff at the Biomolecular Technology Center of the California Institute for Quantitative Biosciences (QB3) at Berkeley for assistance with XPS measurements, D. J. Xiao, A. Turkiewicz, M. E. Ziebel, R. T. Torres-Gavosto and R. Bounds for helpful discussions and experimental assistance, and K. R. Meihaus for editorial assistance.

Author contributions

D.E.J., D.A.R. and J.R.L. formulated the project. D.E.J. and D.A.R. synthesized the materials. D.E.J. and D.A.R. collected and analysed the gas adsorption data. H.Z.H.J. collected and analysed the infrared spectra. D.E.J., J.O. and V.C. collected and analysed the X-ray diffraction data. M.W.M., D.J.L. and D.K.S. collected and analysed the X-ray absorption spectra. A.C.F., M.C. and J.A.R. collected and analysed the NMR spectra. R.A.M. collected and analysed the X-ray photoemission spectroscopy data. D.E.J., D.A.R. and J.R.L. wrote the manuscript, and all authors contributed to revising the manuscript.

Competing interests

The authors declare the following competing interests: J.R.L. has a financial interest in Mosaic Materials, Inc., a start-up company working to commercialize metal–organic frameworks for gas separations. The University of California, Berkeley has applied for a patent on some of the technology discussed herein, on which J.R.L., D.E.J. and D.A.R. are listed as co-inventors.

Additional information

Supplementary information is available for this paper at https://doi.org/10.1038/s41563-019-0597-8.

Correspondence and requests for materials should be addressed to J.R.L.